Mapping Modified Electronic Levels in the Moiré Patterns in MoS 2 /WSe 2 Using Low-Loss EELS

Sandhya Susarla, Lucas M. Sassi, Alberto Zobelli, Steffi y Woo, Luiz Tizei, Odile Stéphan, Pulickel M Ajayan

Mapping modified electronic levels in the moiré patterns in MoS_2/WSe_2 using low-loss EELS

Sandhya Susarla[1,2†], Lucas M. Sassi[1], Alberto Zobelli[2], Steffi Y. Woo[2], Luiz H. G. Tizei[2], Odile Stéphan[2]* and Pulickel M. Ajayan[1]**

1: Department of Materials Science and Nanoengineering, Rice University, Houston, Texas, 77005

2 : Laboratoire de Physique des Solides, Université Paris-Saclay, CNRS, 91405 Orsay, France

* corresponding authors

KEYWORDS: STEM-EELS, moiré excitons, TMDs, van der Waals heterostructures

ABSTRACT

Hybrid/moiré interlayer and intralayer excitons have been realized in twisted two-dimensional transition metal chalcogenides (2D-TMD) due to variation in local moiré potential within a moiré supercell. Though, moiré excitons have been detected in TMD heterostructures by macroscopic spectroscopic techniques, their spatial distribution is experimentally unknown. In the present work, using high-resolution scanning transmission electron microscopy (STEM) and electron energy-loss spectroscopy (EELS), we explore the effect of the twist angle in MoS_2/WSe_2 heterostructures. We observe weak interaction between the layers at higher twist

angles (> 5º) and stronger interaction for lower twist angles. The optical response of the heterostructure varies within the moiré supercell, with a lower energy absorption peak appearing in regions with the AA stacking.

TEXT

"Twistronics" has emerged as an upcoming and promising way to manipulate two-dimensional (2D) materials for applications in quantum computing.[1–6] Stacking two monolayer 2D materials with deliberate rotational misalignment generates a new periodic arrangement known as a moiré pattern. In materials like graphene and hexagonal boron nitride (h-BN), moiré patterns introduce controllable periodic potentials resulting in the generation of flat electronic bands, for example with Hofstadter's butterfly spectral signatures,[7] or at the origin of Mott insulator states in graphene-h-BN heterostructures[8] or emergent properties like superconductivity in magic twist angle in bi-layer graphene.[2]

Similarly, moiré patterns have created interesting effects in transition metal dichalcogenides (TMDs) which are MX_2 type compounds where M = Mo/W, X = S/Se/Te, etc.[1,3,4,6,9–15] Semiconducting monolayer TMDs have large excitonic binding energies, making them observable even at room temperature.[14] Additionally, TMDs heterostructures could have lower energy interlayer excitons arising from bands having the same spin characters at different layers.[15] Artificial stacking of such TMDs gives an additional degree of freedom to control these interlayer excitons by changing the twist angle.[4] However, given the typical exciton radius of TMDs (~1 nm scale), the moiré effects can only be observed when their periodicity is large. It has been demonstrated both theoretically and experimentally that at specific twist angles (< 5º) moiré mini bands are generated that result in the formation of moiré/hybridized excitons in

vertical TMD heterostructures.[1,4,11,13,16–18] These moiré/hybridized excitons can be controlled by circularly polarized light, electrical biasing and magnetic field.[3,4]

Most experiments probing such excitons are based on optical absorption, reflectivity or photoluminescence, with a lower limit for spatial resolution defined by diffraction and typically of the $\lambda/2$ scale (above 500 nm). Therefore, up to now, local effects of the moiré periodicity have only been probed indirectly. On the other hand, scanning probe techniques, such as STS (scanning tunneling spectroscopy) or EELS (electron energy loss spectroscopy) using a focused electron probe in a STEM (scanning transmission electron microscope) can measure spectral information with sub-nanometer spatial resolution. EELS measures the inelastic electron scattering giving information about different neutral excitations in materials, such as excitons, plasmons and core-level excitations.[19] Recent advances in electron optics have made it possible to achieve spectral resolution in the tens of meV scale[20–24] in conjunction to high spatial resolution (sub-1 nm), making it a one of a kind technique to obtain spectral information at the atomic scale.[22] Very recently, Gogoi et. al. have understood the interlayer couplings in moiré MoS_2/WSe_2 heterostructures above room temperatures using EELS spectroscopy.[25] Similarly, using STS, Pan et. al[18] and Zhang et. al.[16] has measured the additional electronic states at the at the top (bottom) of the valence (conduction) band at the Γ (K) points in the moiré MoS_2/WSe_2 heterostructure.

In this letter, we have utilized the advantageous spatial and spectral resolution in EELS to image the interlayers excitons in MoS_2/WSe_2 moiré heterostructure at low temperatures (~120 K). We have observed that the MoS_2/WSe_2 heterostructure EELS spectra are dependent on twist angles. High angle structures (close to 30° rotation) show spectra that resemble pure MoS_2 and WSe_2 (with substantial damping of the WSe_2 contribution). Low angle structures (close to 0°

rotation) are very different, probably due to strong hybridization between the two layers. In these low angle structures, we observe indications of a low energy interlayer exciton at specific points of the moiré pattern.

Results and discussion:

MoS_2 and WSe_2 were individually grown by chemical vapor deposition (CVD). Heterostructures of MoS_2/WSe_2 were formed by stacking the individual layers by PDMS dry transfer and subsequently transferring the heterostructure assembly on Mo quantifoil TEM grids by wet transfer. Details are given in the supplementary information. Figure 1a (inset) shows the low magnification scanning transmission electron microscope (STEM) image of the MoS_2/WSe_2 heterostructure with hexagonal flakes being WSe_2 and the remaining large area being MoS_2. The different twist angles of as-transferred heterostructures were determined by nano-diffraction (Figure S2, Figure 1b,c). All the EELS experiments were performed at low temperatures (~120 K) to study low temperature interlayer excitations. Figure 1a displays the EELS spectra of monolayer MoS_2 and WSe_2 and their heterostructures with aligned (0.3° degree twist) and anti-aligned (30° degree twist) configurations. For a thin material, low-loss EELS measures the imaginary part of the dielectric function[26] and can be directly compared to optical absorption. In the present experiment, MoS_2 monolayer displays two spin-split exciton peaks ($X_{A,Mo}$ and $X_{B,Mo}$) at 1.96 eV and 2.15 eV whereas the intralayer exciton for WSe_2 ($X_{A,W}$ and $X_{B,W}$) were found at 1.75 eV and 2.3 eV. We found that the intralayer exciton peak for MoS_2 or WSe_2 were above or below the reported optical absorption values at 150 K.[27–29] We suspect that this variation could result from local strain or presence of defects.[30,31] However, the exciton peaks of intrinsic MoS_2 and WSe_2 monolayers match with the ones measured by earlier EELS studies.[24] The linewidth of

WSe_2 is significantly larger than that of MoS_2, possibly due to a higher defect concentration in the WSe_2 layer.

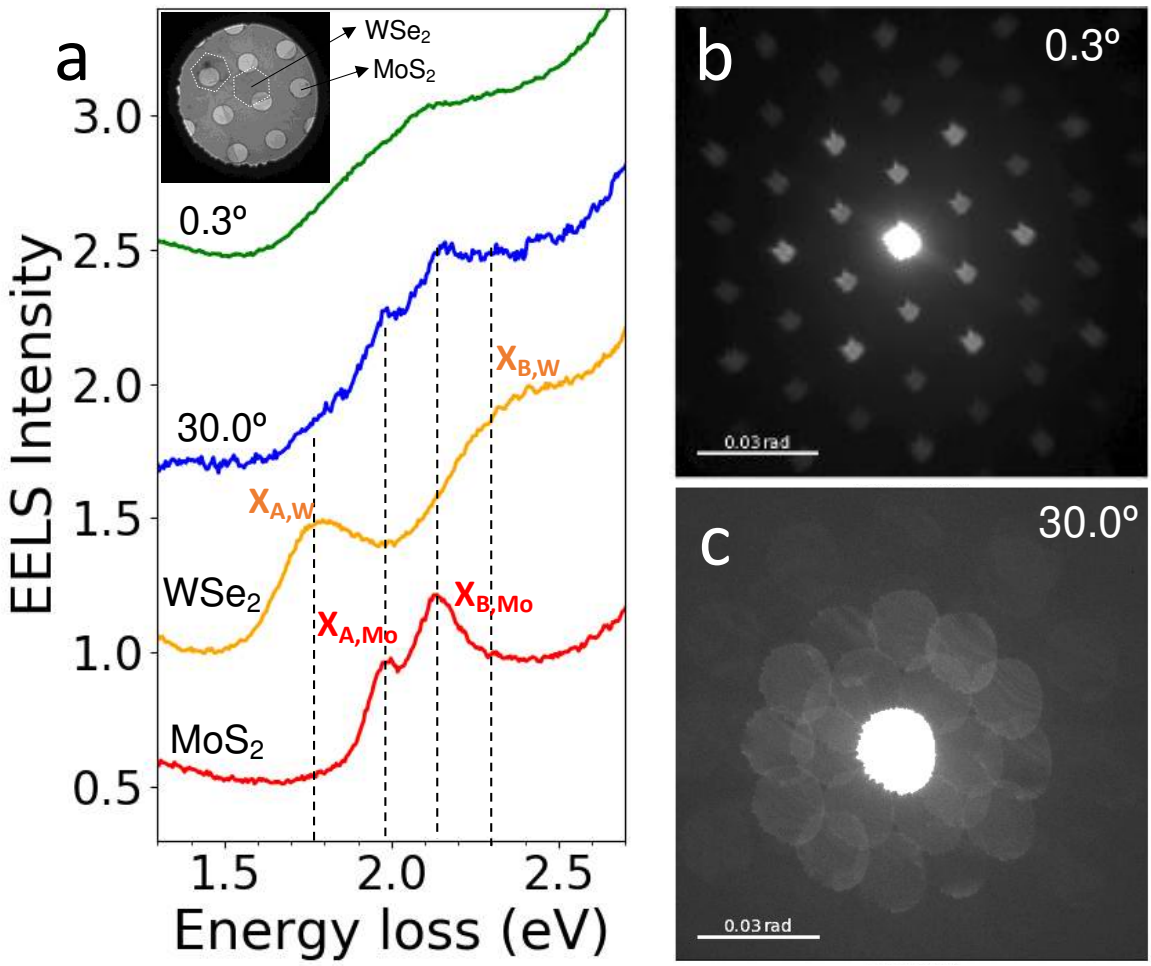

Figure 1. EELS spectroscopy of MoS_2/WSe_2 heterostructures. a) Average EELS spectrum of MoS_2, WSe_2 and MoS_2/WSe_2 heterostructures at anti-aligned (30°) and aligned (0.3°), respectively. Nanodiffraction of b) 0.3° and c) 30° twisted heterostructures. The zero-background of the peak is indicated by dashed horizontal black lines. The onset, indicated at the black solid vertical line, is at the point where the spectrum is just above the background. (presented by a horizontal line).

With the knowledge on intrinsic intralayer excitons in MoS_2 and WSe_2, we now understand the exciton absorption in MoS_2/WSe_2 heterostructures. In anti-aligned heterostructures (30° twist), there are three distinct peaks (1.74 eV, 1.93 eV and 2.08 eV) observed at similar energies to

$X_{A,W}$, $X_{A,Mo}$ and $X_{B,Mo}$ respectively. The three excitonic lines observed at similar energies to those in the intrinsic monolayers suggest a weak interaction between the layers for this configuration. However, the peak at the WSe_2-related $X_{A,W}$ is weaker than the other two, indicating that the optical response is influenced by the heterostructure.

In sharp contrast, EELS spectra of the aligned heterostructure (0.3° twist), is broader with a lower energy onset (~1.6 eV) than the $X_{A,W}$ peak in the anti-aligned heterostructure configuration indicating a significant modification of the optical response due to the moiré pattern. Since, the spectrum here is averaged out over a large (50 nm) region, a distinct moiré exciton peak is not observed unlike in previous optical spectroscopy studies.[3,4,11] It is to be noted that the width of the all the EELS peaks are broader than the ones measured by confocal optical spectroscopy techniques. This is probably due to presence of native defects in the CVD grown intrinsic MoS_2 and WSe_2 monolayers used to produce the heterostructures. Furthermore, as-transferred samples used in the this experiment have not been encapsulated within h-BN layers, a technique which has been demonstrated to be very effective in preserving the optical response of 2D materials by strongly limiting their aging effect.[11,32]

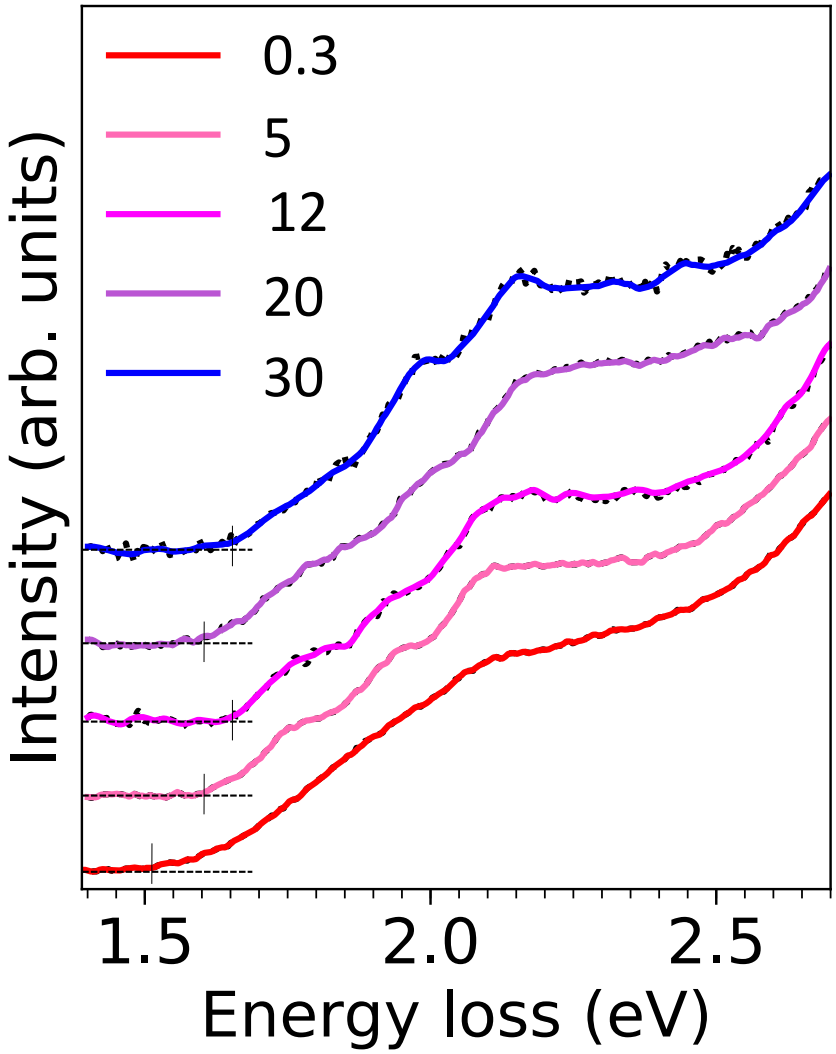

Figure 2. Average and smoothed EELS spectra of MoS_2/WSe_2 heterostructures with different twist angle. The zero-background of the peak is indicated by dashed horizontal black lines. The onset, indicated at the black solid vertical line, is at the point where the spectrum is just above the background.

To have a better understanding of how these interlayer excitations depend on the twist angle, EELS was repeated in multiple areas with different twist angle (Figure 2). Spectra have been smoothed using the Savitzky-Golay algorithm (implemented in the Scipy library of Python).[33] Energy positions (Table 1) of the peaks have been extracted from fits to the second derivative of the smoothed spectra extracted using the same algorithm (Figure S4).

Moiré angle	**$X_{A,W}$ (eV)**	**$X_{A,Mo}$ (eV)**	**$X_{B,Mo}$ (eV)**
0.3 degree		1.87	2.10
5 degree	1.75	1.93	2.10
12 degrees	1.76	1.93	2.11
21 degrees	1.77	1.97	2.19
30 degrees	1.75	1.96	2.16
MoS_2		1.96	2.15
WSe_2	1.75		

Table 1. EELS peaks position derived gaussian fits from their respective second derivative spectra. The typical standard deviation of the peak center fitting coefficient was between 1-4 meV. These uncertainties are added to possible variations due to sample heterogeneity, as discussed in the main text.

From Figure 2 and Table 1 two key observations can be extracted. First, the intralayer excitons peaks associated to $X_{A,W}$, $X_{A,Mo}$ and $X_{B,Mo}$ remain invariant at higher twist angles ($5<\boldsymbol{\theta}<30$) at 1.76 ± 0.01 eV, 1.94 ± 0.02 eV and 2.14 ± 0.02 eV respectively. The few tens of meV variation in exciton absorption is likely due to variation in strain and defect density.[31] The intralayer exciton energies for heterostructures are similar to intrinsic intralayer excitons for monolayer MoS_2 and WSe_2 respectively implying less/no coupling at higher twist angles. Second, there is an early onset for the EELS absorption at the nearly aligned heterostructure. We also observe a significant broadening of the spectra. We suspect that this early onset is due to the stronger interaction between MoS_2 and WSe_2 for nearly aligned configuration. Since the overall EELS spectra for lower angles is broader than those with higher angles, we are unable to draw conclusions about specific exciton peak shift. However, our observation of an early EELS onset agrees with the previous reports on the rotation dependence of both the interlayer and intralayer

exciton peaks by photoluminescence, optical reflectance and low-magnification EELS in several TMD heterostructures e.g. $MoSe_2/WS_2$, MoS_2/WSe_2 heterostructures.[3,11,25]

Contrary to widely used optical techniques, EELS can measure the spectroscopic response at a very high spatial resolution, below the optical diffraction limit but this capability has not yet been employed in the case of TMD moiré heterostructures on which notable spatial variations might exists. The perturbation theory Wu et. al. has proposed that the periodic moiré potential produces changes in the local registry of atoms which ultimately influence the interlayer exciton dynamics.[34] The periodic potential splits the interlayer excitons into independent eigen states which tend to be confined at the proximity of potential minima at high symmetry points of the moiré lattice.[3,4,6,12,13,34] Low angle moiré patterns between MoS_2 and WSe_2 correspond to supercells having a period larger than the typical exciton radius for TMDs (~1nm) which might lead to spatially varying exciton spectra. In order to understand the spatial variation in the excitons strong-coupling regime or nearly aligned configuration, it is important to first understand the local configuration within one moiré supercell in the MoS_2/WSe_2 heterostructures. Several quasi high symmetry local stacking orders can occur within the moiré lattice. In two configurations the hexagons overlaps: (i) AA, Mo on top of W and S on top of Se, and (ii) AA', Mo on top of Se and W on top of S. Four configurations present a Bernal type stacking which can be notated as (iii) AB_{Se}^{Mo}, (iv) AB_{W}^{S}, (v) AB_{W}^{Mo}, (vi) AB_{Se}^{S} where the atomic species at the top layer and bottom layer overlap at the β sites (where two atoms stack vertically) which do not explicitly occur at the center of the hexagon of the adjacent layer. In low twist angle moiré structures, it is possible to find the spatially separated AA, AB_{W}^{S} , AB_{Se}^{Mo} configurations by a simple plane glide. However, in moiré structures with twist angles close to 30° the AA', AB_{W}^{Mo}, and AB_{Se}^{S} structures can be overlapped. In between these high symmetry

configurations, there are regions where the atoms of one layer lie in a bridge position with respect to the atoms of the adjacent layer (a general seventh configuration here identified as Br).

From a rigorous crystallographic point of view, a moiré super period occurs only when the two layers have commensurable lattices. However, even when this strict condition is not satisfied, quasi-high symmetry stacking regions are regularly distributed across the heterostructure and a moiré-like structure arises. This effect has been extensively discussed to explain the triangular patterns observed in STM images[35,36] and analogous considerations can be applied to the case of STEM images. Furthermore, moiré superstructures with slightly different twist angles could present very different periods but the distance between high symmetry stacking regions and the associated apparent period do not drastically change.[35]

Figure 3a shows a high angle annular dark field (HAADF) image of a MoS_2/WSe_2 heterostructure where equivalent brighter regions are about 14 nm apart. Figure 3b shows the associated nano-diffraction pattern from which a twist angle of 0.3±0.1° and a lattice mismatch of 2.3±0.9% can be derived. Bulk lattice parameters differ by about 4%, but this discrepancy can be lowered by deformations induced by interlayer coupling. The strain caused by the lattice mismatch will induce energy shifts of the excitonic lines of both materials, with compressive /tensile strain leading to blue/red shifts, respectively. Both uniaxial[37–39] and biaxial[40] strain lead to similar behavior in TMD monolayers, with different amplitudes of energy shift for a given strain percentage. These values are in accordance with the pattern observed in HAADF images. Indeed, the very low twist angle imposes that the apparent period would be very close to those obtained for aligned layers. The measured lattice mismatch defines a superperiod corresponding to $n+1$ MoS_2 unit cells over n WSe_2 unit cells with n approximately equal to 40. Using the

experimentally observed lattice mismatch (δ), moiré angle (θ) and bulk lattice parameters of MoS_2 (a), the expected moiré period (L) was determined from the following equation.[41]

$$L = \frac{(1+\delta)a}{\sqrt{\delta^2 + 2(1+\delta)(1-\cos\theta)}}$$

The expected moiré periodicity, 13.5 nm, is in good agreement with the HAADF images. The measured lattice mismatch, 2.3 %, is crucial to match the correct structure, as the bulk mismatch of 4% leads to a smaller moiré period (8.6 nm). (Figure S6)

An atomic model of an heterostructure formed by aligning and overlapping (41×41) MoS_2 and (40×40) WSe_2 supercells is given in Figure 3c, where the location of high symmetry configurations has been highlighted. These local structures can be clearly identified in the Figure 3a. Regions indicated by the correspondingly-colored rectangles have been magnified in Figure 3d-g. In HAADF images, each illuminated atom provides a signal which depends on its atomic number ($\propto Z^{1.6}$) and therefore the technique allows us to easily discriminate heavy and light atomic species. The three high symmetry configurations expected for a low angle twist can then be identified in the Figure 3c. For the AA configuration, the bright and dark atomic columns correspond to the superposition of the metal and chalcogen atoms respectively (Figure 3d). In the AB_{Se}^{Mo} configuration, the intensity derived from the overlapping of a Mo and two Se atoms is very close to those of the W atom while the much lighter sulfur atoms make minimal contribution to the image intensity (Figure 3e). In the AB_{W}^{S}, the brighter triangular lattice is formed by the overlap of W and S atoms while the intensity of Mo and the two Se sites is very similar (Figure 3f). The intermediate bridge positions can also be imaged (Figure 3g). This allows a direct connection between the observed intensity patterns observed at low magnification

with the local atomic stacking: bright, medium, and dark intensity spots correspond to AB_{Se}^{Mo}, AA, and AB_{W}^{S} configuration, respectively.

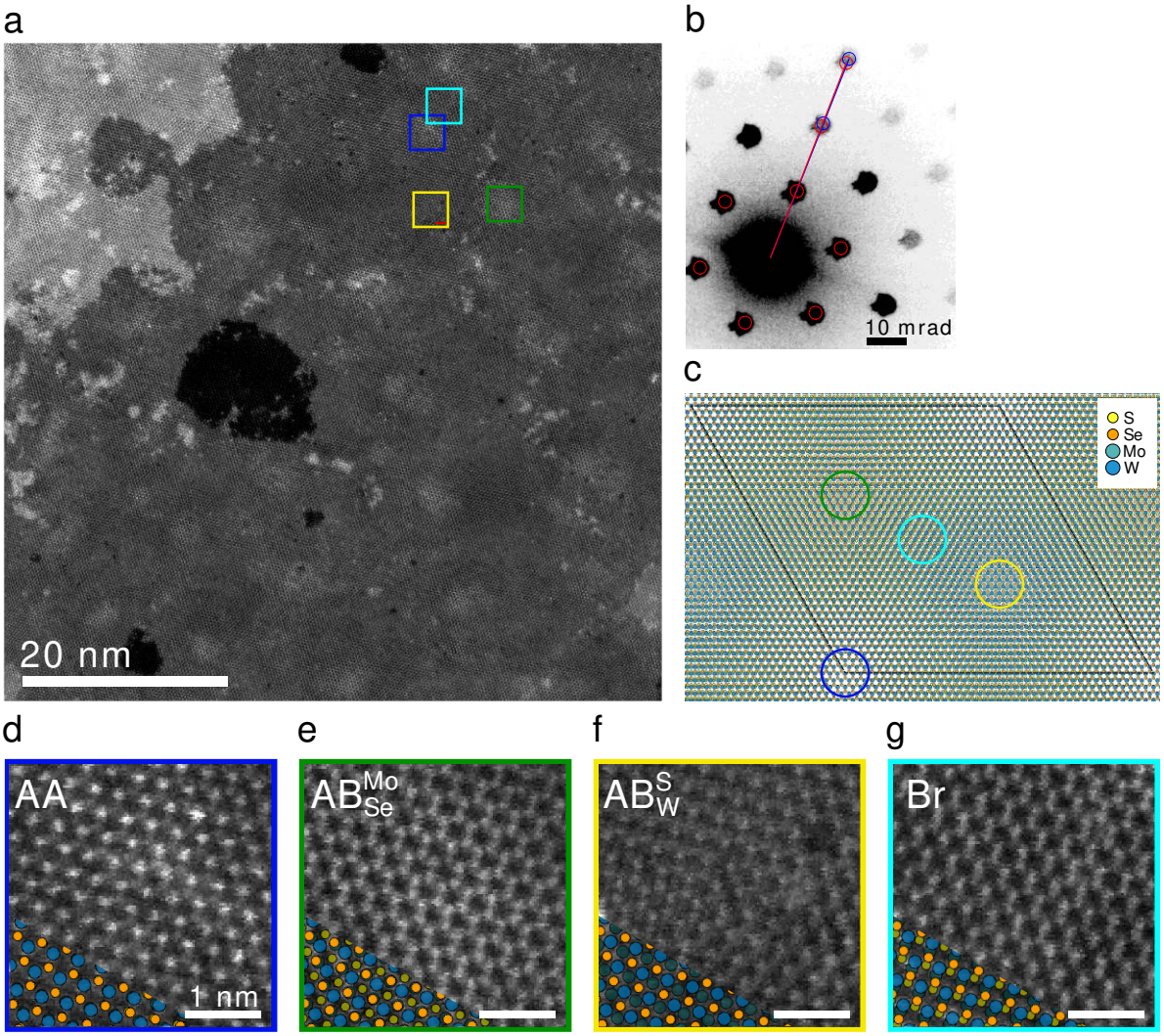

Figure 3. Identification of atomic configuration within one moiré supercell. a) Large field of view HAADF image of a low angle moiré structure with period 14 nm. b) Diffraction pattern of the region, showing the two diffraction patterns of the two monolayers almost perfectly superposed. Differences can only be seen for higher order reflections. c) Schematics of the moiré pattern formed when MoS_2 and WSe_2 are aligned with 0.3° rotation. The difference in the lattice parameter between the two materials result in 14 nm moiré period. Within the moiré supercell, there are four configurations whose zoomed-in images are displaced in d-g.

After identifying all the configurations, STEM-EELS mapping at cryogenic temperature (120 K) was carried out to map the optical response of different moiré structures. Mapping was

performed in raster mode wherein each pixel of the image corresponds to an EELS spectrum as a hyperspectral image. Figure 4a shows a medium angle annular dark field (MAADF) image of the heterostructure, with the white rectangle marking the region where the hyperspectral image was acquired. The image displays three intensity levels of bright, medium, and dark. From the relation between structure and intensity in images shown in Figure 3, we attribute bright, medium, and dark regions to AB_{Se}^{Mo}, AA, and AB_{W}^{S} configurations, respectively

Here we will focus on the low energy part of the spectra, where an interlayer exciton has been observed in previous works.[16,18] STS experiments have observed a decrease of the band gap and the appearance of lower energy states with respect to the conduction band, confined to specific positions of a moiré superlattice.[16,18] Figure 4d shows the representative EELS spectra collected from regions of three different levels of intensity (bright, medium and dark) from a different location to Figure 3. Spectra (marked red, green and blue) were extracted from the equivalent sites (16x16 pixels each) marked in Figure 4b, where the moiré pattern is periodic. Ten equivalent sites from the bright, medium and dark intensity were summed up for EELS spectra. (EELS spectra summed up=10x16x16 pixels) For the medium intensity region or AA configuration (green square in Figure 4b), we observe a slight decrease of the absorption onset and the appearance of a minor absorption peak; attributed to additional electronic levels. Magnified spectra from 1.4-1.8 eV range is described in inset. Details of the background subtraction are presented in supplementary information (Figure S7). According to the previous optical reflectance and PL studies, the onset of absorption on semiconducting transition metal dichalcogenides is given by an excitonic transition.[3,4,6,10,11] The additional electronic levels at zero degree moiré closely matches with momentum space indirect exciton reported by Kunstmann et. al. (PL and DFT calculations).[10] Further, from the filtered maps (1.4-1.6 eV

energy range) in Figure 4e, it can be observed that the broad minor absorption peak is mostly confined to medium spots or AA configuration. We also do observe a weak signal from the dark spots. The small peak occurring at the medium intensity locations disappears in a disordered arrangement of bright, medium or dark intensity.

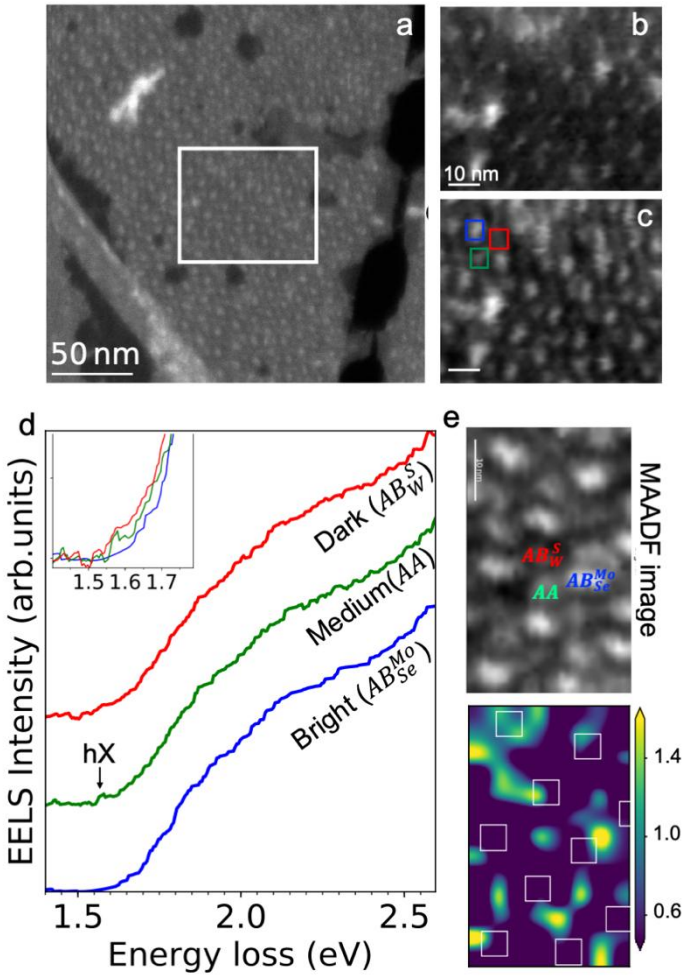

Figure 4. High resolution EELS maps of nearly aligned (0.3 degree) MoS2/WSe2 heterostructure. a) low magnification MAADF image of the moiré pattern. The white rectangle marks the region where the hyperspectral image was acquired. b-c) ADF and MAADF images, respectively, acquired with a hyperspectral image on the moiré structure. d) EELS spectra averaged over multiple equivalent sites of the bright or AB_{Se}^{Mo} (blue square), medium or AA (green square) and dark or AB_W^S (red square) intensity regions in the MAADF image. The EELS comparison plot shown on the below is sum of EELS spectra extracted from ordered arrangement of bright (AB_{Se}^{Mo}), medium (AA) and dark (AB_W^S) intensity regions. Inset shows the zoomed in spectrum from 1.4-1.8 eV. e) MAADF image and the corresponding energy filtered map from the 1.4-1.6 eV energy window. The bright spots from MAADF image are marked as

white squares in the filtered maps. The additional electronic levels are observed prominently in the medium regions of the MAADF image. The map was normalized by the total intensity in the EEL spectrum to avoid diffraction effects in the filtered maps presented.

Conclusions:

In conclusion, we have observed that in moiré structures formed by MoS_2 and a WSe_2 monolayers the onset of the EELS spectral response can be modified by the twist angle between the two layers. The low angle structures (0.3°) are strongly coupled, while the higher angle ones (30°) behave almost as independent layers. Furthermore, for a nearly aligned configuration (0.3° twist angle) an additional shallow peak appears near the adsorption edge. This spectral feature is mostly localized to *AA* regions of the moiré MAADF images and can be tentatively assigned to an interlayer moiré exciton

ASSOCIATED CONTENT

TOC Figure:

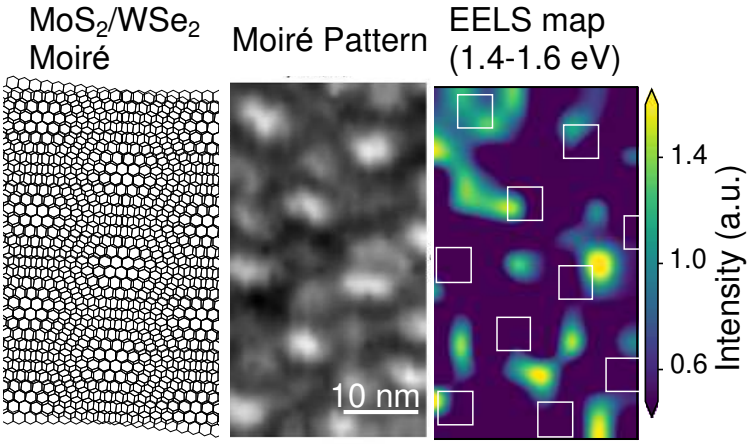

Supporting Information.

The following files are available free of charge.

experimental methods and supporting figures (Supplementary information.pdf)

AUTHOR INFORMATION

Corresponding Author

*Luiz H. G. Tizei Laboratoire de Physique des Solides, Université Paris-Saclay, CNRS, 91405 Orsay, France; ORCID:orcid.org/0000-0003-3998-9912; Email: luiz.galvao- tizei@u-psud.fr

* Odile Stephan −Laboratoire de Physique des Solides, Université Paris-Saclay, CNRS, 91405 Orsay, France; Email: odile.stephan@u-psud.fr

* Pulickel M. Ajayan – Materials Science and Nanoengineering, Rice University, Houston, Texas, 77005, Email: ajayan@rice.edu

Authors:

Sandhya Susarla- Materials Science and Nanoengineering, Rice University, Houston, Texas, 77005, ORCID: https://orcid.org/0000-0003-1773-0993

Lucas M. Sassi- Materials Science and Nanoengineering, Rice University, Houston, Texas, 77005.

Alberto Zobelli − Laboratoire de Physique des Solides, Université Paris-Saclay, CNRS, 91405 Orsay, France.

Steffi Y. Woo- Laboratoire de Physique des Solides, Université Paris-Saclay, CNRS, 91405 Orsay, France.

Present Addresses

† Materials Science Division, Lawrence Berkeley National Laboratory

Author Contributions

S.S prepared the microscopy samples, performed HAADF imaging, analyzed most HAADF and EELS data and participated in EELS experiments. L.S. grew the CVD samples and made the MoS_2/WSe_2 heterostructure assembly. A.Z. analyzed the moiré structure of MoS_2/WSe_2 and was involved extensively in STEM-EELS technical discussion. S.Y.W helped in the technical discussion and EELS experiments. L.H.G.T. performed the EELS experiments and helped in EELS data analysis. L.H.G, O.S and P.MA conceived the idea and supervised the overall project. SS, L.S, LH.G.T and A.Z co-wrote the manuscript. All authors have given approval to the final version of the manuscript.

ACKNOWLEDGMENT

This material is based upon research supported by the Chateaubriand Fellowship of the Office for Science & Technology of the Embassy of France in the United States. This project was partially funded by the National Agency for Research under the program of future investment TEMPOS-CHROMATEM (reference no. ANR-10-EQPX-50). L.M.S. acknowledges CAPES (Coordination for the Improvement of Higher Education Personnel), sponsored by the Brazilian Ministry of Education, for financial support.

REFERENCES

.(1) Yu, H.; Liu, G.-B.; Tang, J.; Xu, X.; Yao, W. Moiré Excitons: From Programmable Quantum Emitter Arrays to Spin-Orbit–Coupled Artificial Lattices. *Sci. Adv.* **2017**, *3* (11), e1701696.

(2) Cao, Y.; Fatemi, V.; Fang, S.; Watanabe, K.; Taniguchi, T.; Kaxiras, E.; Jarillo-Herrero, P. Unconventional Superconductivity in Magic-Angle Graphene Superlattices. *Nature*

2018, *556* (7699), 43.

(3) Seyler, K. L.; Rivera, P.; Yu, H.; Wilson, N. P.; Ray, E. L.; Mandrus, D. G.; Yan, J.; Yao, W.; Xu, X. Signatures of Moiré-Trapped Valley Excitons in MoSe 2/WSe 2 Heterobilayers. *Nature* **2019**, *567* (7746), 66.

(4) Jin, C.; Regan, E. C.; Yan, A.; Utama, M. I. B.; Wang, D.; Zhao, S.; Qin, Y.; Yang, S.; Zheng, Z.; Shi, S. Observation of Moiré Excitons in WSe 2/WS 2 Heterostructure Superlattices. *Nature* **2019**, *567* (7746), 76.

(5) Shimazaki, Y.; Schwartz, I.; Watanabe, K.; Taniguchi, T.; Kroner, M.; Imamoğlu, A. Strongly Correlated Electrons and Hybrid Excitons in a Moiré Heterostructure. *Nature* **2020**, *580* (7804), 472–477.

(6) Tran, K.; Moody, G.; Wu, F.; Lu, X.; Choi, J.; Kim, K.; Rai, A.; Sanchez, D. A.; Quan, J.; Singh, A. Evidence for Moiré Excitons in van Der Waals Heterostructures. *Nature* **2019**, *567* (7746), 71.

(7) Dean, C. R.; Wang, L.; Maher, P.; Forsythe, C.; Ghahari, F.; Gao, Y.; Katoch, J.; Ishigami, M.; Moon, P.; Koshino, M.; et al. Hofstadter's Butterfly and the Fractal Quantum Hall Effect in Moiré Superlattices. *Nature* **2013**, *497* (7451), 598–602.

(8) Chen, G.; Jiang, L.; Wu, S.; Lyu, B.; Li, H.; Chittari, B. L.; Watanabe, K.; Taniguchi, T.; Shi, Z.; Jung, J. Evidence of a Gate-Tunable Mott Insulator in a Trilayer Graphene Moiré Superlattice. *Nat. Phys.* **2019**, *15* (3), 237.

(9) Ulstrup, S.; Koch, R. J.; Singh, S.; McCreary, K. M.; Jonker, B. T.; Robinson, J. T.;

Jozwiak, C.; Rotenberg, E.; Bostwick, A.; Katoch, J. Direct Observation of Minibands in a Twisted Graphene/WS2 Bilayer. *Sci. Adv.* **2020**, *6* (14), eaay6104.

(10) Kunstmann, J.; Mooshammer, F.; Nagler, P.; Chaves, A.; Stein, F.; Paradiso, N.; Plechinger, G.; Strunk, C.; Schüller, C.; Seifert, G.; et al. Momentum-Space Indirect Interlayer Excitons in Transition-Metal Dichalcogenide van Der Waals Heterostructures. *Nat. Phys.* **2018**, *14* (8), 801–805.

(11) Alexeev, E. M.; Ruiz-Tijerina, D. A.; Danovich, M.; Hamer, M. J.; Terry, D. J.; Nayak, P. K.; Ahn, S.; Pak, S.; Lee, J.; Sohn, J. I. Resonantly Hybridized Excitons in Moiré Superlattices in van Der Waals Heterostructures. *Nature* **2019**, *567* (7746), 81.

(12) Yu, H.; Wang, Y.; Tong, Q.; Xu, X.; Yao, W. Anomalous Light Cones and Valley Optical Selection Rules of Interlayer Excitons in Twisted Heterobilayers. *Phys. Rev. Lett.* **2015**, *115* (18), 187002.

(13) Wu, F.; Lovorn, T.; MacDonald, A. H. Topological Exciton Bands in Moiré Heterojunctions. *Phys. Rev. Lett.* **2017**, *118* (14), 147401.

(14) Kylänpää, I.; Komsa, H.-P. Binding Energies of Exciton Complexes in Transition Metal Dichalcogenide Monolayers and Effect of Dielectric Environment. *Phys. Rev. B* **2015**, *92* (20), 205418.

(15) Rivera, P.; Yu, H.; Seyler, K. L.; Wilson, N. P.; Yao, W.; Xu, X. Interlayer Valley Excitons in Heterobilayers of Transition Metal Dichalcogenides. *Nat. Nanotechnol.* **2018**, *13* (11), 1004–1015.

(16) Zhang, C.; Chuu, C.-P.; Ren, X.; Li, M.-Y.; Li, L.-J.; Jin, C.; Chou, M.-Y.; Shih, C.-K. Interlayer Couplings, Moiré Patterns, and 2D Electronic Superlattices in MoS2/WSe2 Hetero-Bilayers. *Sci. Adv.* **2017**, *3* (1), e1601459.

(17) Ruiz-Tijerina, D. A.; Fal'ko, V. I. Interlayer Hybridization and Moiré Superlattice Minibands for Electrons and Excitons in Heterobilayers of Transition-Metal Dichalcogenides. *Phys. Rev. B* **2019**, *99* (12), 125424.

(18) Pan, Y.; Fölsch, S.; Nie, Y.; Waters, D.; Lin, Y.-C.; Jariwala, B.; Zhang, K.; Cho, K.; Robinson, J. A.; Feenstra, R. M. Quantum-Confined Electronic States Arising from the Moiré Pattern of MoS2–WSe2 Heterobilayers. *Nano Lett.* **2018**, *18* (3), 1849–1855.

(19) Kapetanakis, M. D.; Zhou, W.; Oxley, M. P.; Lee, J.; Prange, M. P.; Pennycook, S. J.; Idrobo, J. C.; Pantelides, S. T. Low-Loss Electron Energy Loss Spectroscopy: An Atomic-Resolution Complement to Optical Spectroscopies and Application to Graphene. *Phys. Rev. B* **2015**, *92* (12), 125147.

(20) Lagos, M. J.; Trügler, A.; Hohenester, U.; Batson, P. E. Mapping Vibrational Surface and Bulk Modes in a Single Nanocube. *Nature* **2017**, *543* (7646), 529–532.

(21) Krivanek, O. L.; Lovejoy, T. C.; Dellby, N.; Aoki, T.; Carpenter, R. W.; Rez, P.; Soignard, E.; Zhu, J.; Batson, P. E.; Lagos, M. J. Vibrational Spectroscopy in the Electron Microscope. *Nature* **2014**, *514* (7521), 209–212.

(22) Kociak, M.; Gloter, A.; Stéphan, O. A Spectromicroscope for Nanophysics. *Ultramicroscopy* **2017**, *180*, 81–92.

(23) Krivanek, O. L.; Ursin, J. P.; Bacon, N. J.; Corbin, G. J.; Dellby, N.; Hrncirik, P.; Murfitt, M. F.; Own, C. S.; Szilagyi, Z. S. High-Energy-Resolution Monochromator for Aberration-Corrected Scanning Transmission Electron Microscopy/Electron Energy-Loss Spectroscopy. *Philos. Trans. R. Soc. A Math. Phys. Eng. Sci.* **2009**, *367* (1903), 3683–3697.

(24) Tizei, L. H. G.; Lin, Y.-C.; Mukai, M.; Sawada, H.; Lu, A.-Y.; Li, L.-J.; Kimoto, K.; Suenaga, K. Exciton Mapping at Subwavelength Scales in Two-Dimensional Materials. *Phys. Rev. Lett.* **2015**, *114* (10), 107601.

(25) Gogoi, P. K.; Lin, Y.-C.; Senga, R.; Komsa, H.-P.; Wong, S. L.; Chi, D.; Krasheninnikov, A. V; Li, L.-J.; Breese, M. B. H.; Pennycook, S. J.; et al. Layer Rotation-Angle-Dependent Excitonic Absorption in van Der Waals Heterostructures Revealed by Electron Energy Loss Spectroscopy. *ACS Nano* **2019**, *13* (8), 9541–9550.

(26) Kociak, M.; Kasumov, A. Y.; Guéron, S.; Reulet, B.; Khodos, I. I.; Gorbatov, Y. B.; Volkov, V. T.; Vaccarini, L.; Bouchiat, H. Superconductivity in Ropes of Single-Walled Carbon Nanotubes. *Phys. Rev. Lett.* **2001**, *86* (11), 2416–2419.

(27) Zhang, C.; Wang, H.; Chan, W.; Manolatou, C.; Rana, F. Absorption of Light by Excitons and Trions in Monolayers of Metal Dichalcogenide Mo S 2: Experiments and Theory. *Phys. Rev. B* **2014**, *89* (20), 205436.

(28) Arora, A.; Wessling, N. K.; Deilmann, T.; Reichenauer, T.; Steeger, P.; Kossacki, P.; Potemski, M.; Michaelis de Vasconcellos, S.; Rohlfing, M.; Bratschitsch, R. Dark Trions Govern the Temperature-Dependent Optical Absorption and Emission of Doped

Atomically Thin Semiconductors. *Phys. Rev. B* **2020**, *101* (24), 241413.

(29) Arora, A.; Koperski, M.; Nogajewski, K.; Marcus, J.; Faugeras, C.; Potemski, M. Excitonic Resonances in Thin Films of WSe 2: From Monolayer to Bulk Material. *Nanoscale* **2015**, *7* (23), 10421–10429.

(30) Moon, H.; Bersin, E.; Chakraborty, C.; Lu, A.-Y.; Grosso, G.; Kong, J.; Englund, D. Strain-Correlated Localized Exciton Energy in Atomically Thin Semiconductors. *ACS Photonics* **2020**, *7* (5), 1135–1140.

(31) Kolesnichenko, P. V; Zhang, Q.; Yun, T.; Zheng, C.; Fuhrer, M. S.; Davis, J. A. Disentangling the Effects of Doping, Strain and Disorder in Monolayer WS2 by Optical Spectroscopy. *2D Mater.* **2020**, *7* (2), 25008.

(32) Thiel, L.; Wang, Z.; Tschudin, M. A.; Rohner, D.; Gutiérrez-Lezama, I.; Ubrig, N.; Gibertini, M.; Giannini, E.; Morpurgo, A. F.; Maletinsky, P. Probing Magnetism in 2D Materials at the Nanoscale with Single-Spin Microscopy. *Science.* **2019**, *364* (6444), 973 LP – 976.

(33) Virtanen, P.; Gommers, R.; Oliphant, T. E.; Haberland, M.; Reddy, T.; Cournapeau, D.; Burovski, E.; Peterson, P.; Weckesser, W.; Bright, J.; et al. SciPy 1.0: Fundamental Algorithms for Scientific Computing in Python. *Nat. Methods* **2020**, *17*, 261–272.

(34) Wu, F.; Lovorn, T.; MacDonald, A. H. Theory of Optical Absorption by Interlayer Excitons in Transition Metal Dichalcogenide Heterobilayers. *Phys. Rev. B* **2018**, *97* (3), 35306.

(35) Campanera, J. M.; Savini, G.; Suarez-Martinez, I.; Heggie, M. I. Density Functional Calculations on the Intricacies of Moir\'e Patterns on Graphite. *Phys. Rev. B* **2007**, *75* (23), 235449.

(36) Artaud, A.; Magaud, L.; Le Quang, T.; Guisset, V.; David, P.; Chapelier, C.; Coraux, J. Universal Classification of Twisted, Strained and Sheared Graphene Moiré Superlattices. *Sci. Rep.* **2016**, *6* (1), 25670.

(37) Aslan, O. B.; Deng, M.; Heinz, T. F. Strain Tuning of Excitons in Monolayer WSe 2. *Phys. Rev. B* **2018**, *98* (11), 115308.

(38) Schmidt, R.; Niehues, I.; Schneider, R.; Drueppel, M.; Deilmann, T.; Rohlfing, M.; De Vasconcellos, S. M.; Castellanos-Gomez, A.; Bratschitsch, R. Reversible Uniaxial Strain Tuning in Atomically Thin WSe2. *2D Mater.* **2016**, *3* (2), 21011.

(39) Island, J. O.; Kuc, A.; Diependaal, E. H.; Bratschitsch, R.; Van Der Zant, H. S. J.; Heine, T.; Castellanos-Gomez, A. Precise and Reversible Band Gap Tuning in Single-Layer MoSe 2 by Uniaxial Strain. *Nanoscale* **2016**, *8* (5), 2589–2593.

(40) McCreary, A.; Ghosh, R.; Amani, M.; Wang, J.; Duerloo, K.-A. N.; Sharma, A.; Jarvis, K.; Reed, E. J.; Dongare, A. M.; Banerjee, S. K. Effects of Uniaxial and Biaxial Strain on Few-Layered Terrace Structures of MoS2 Grown by Vapor Transport. *ACS Nano* **2016**, *10* (3), 3186–3197.

(41) Yankowitz, M.; Xue, J.; Cormode, D.; Sanchez-Yamagishi, J. D.; Watanabe, K.; Taniguchi, T.; Jarillo-Herrero, P.; Jacquod, P.; LeRoy, B. J. Emergence of Superlattice Dirac Points in Graphene on Hexagonal Boron Nitride. *Nat. Phys.* **2012**, *8* (5), 382–386.